Articles

Cooperative Binding of Monodisperse Anionic Amphiphiles to the i-Face: Phospholipase A2-Paradigm for Interfacial Binding†

Otto G. Berg,*,‡ Bao-Zhu Yu,§ Cherry Chang,§ Karl A. Koehler,§ and Mahendra K. Jain*,§

Department of Chemistry and Biochemistry, University of Delaware, Newark, Delaware 19716, and Department of Molecular Evolution, Uppsala University Evolutionary Biology Center, Uppsala, Sweden

Received February 2, 2004; Revised Manuscript Received April 21, 2004

ABSTRACT: Equilibrium parameters for the binding of monodisperse alkyl sulfate along the i-face (the interface binding surface) of pig pancreatic IB phospholipase A_2 (PLA2) to form the premicellar complexes ($E_i^{\#}$) are characterized to discern the short-range specific interactions. Typically, $E_i^{\#}$ complexes are reversible on dilution. The triphasic binding isotherm, monitored as the fluorescence emission from the single tryptophan of PLA2, is interpreted as a cooperative equilibrium for the sequential formation of three premicellar complexes ($E_i^{\#}$, $i = 1, 2, 3$). In the presence of calcium, the dissociation constant K_1 for the $E_1^{\#}$ complex of PLA2 with decyl sulfate (CMC = 4500 μM) is 70 μM with a Hill coefficient $n_1 = 2.1 \pm 0.2$; K_2 for $E_2^{\#}$ is 750 μM with $n_2 = 8 \pm 1$, and K_3 for $E_3^{\#}$ is 4000 μM with an n_3 value of about 12. Controls show that (a) self-aggregation of decyl sulfate alone is not significant below the CMC; (b) occupancy of the active site is not necessary for the formation of $E_i^{\#}$; (c) K_i and n_i do not change significantly due to the absence of calcium, possibly because alkyl sulfate does not bind to the active site of PLA2; (d) the $E_i^{\#}$ complexes show a significant propensity for aggregation; and (e) PLA2 is not denatured in $E_i^{\#}$. The results are interpreted to elaborate the model for atomic level interactions along the i-face: The chain length dependence of the fit parameters suggests that short-range specific anion binding of the headgroup is accompanied by desolvation of the i-face of $E_i^{\#}$. We suggest that allosteric activation of PLA2 results from such specific interactions of the amphiplies and the desolvation of the i-face. The significance of these primary interfacial binding events and the coexistence of the E* and $E_i^{\#}$ aggregates is discussed.

The paradigm for the interfacial binding is conceptualized in Figure 1. Apparently, only one branch is sufficient for the tight binding of PLA2 to the anionic phsopholipid vesicles (*1*, *2*): E* complex on the bilayer is formed because the concentration of the monodisperse amphiphiles is $<10^{-12}$ M; also, E* does not disrupt the integrity of the vesicles and substantially change the bilayer organization, which in effect rules out the possibility of aggregate formation. Such features are critical for the analysis of the interfacial turnover where the reaction path is unequivocally defined (*1*). However, understanding short-range specific interactions of amphiphile headgroups along the interface binding surface (i-face[11]) of E* is a challenging problem (*1*−*11*), principally because the amphiphiles in contact with the i-face are not readily amenable to experimental and analytical manipulations. To circumvent such difficulties we have recently shown that distinct premicellar complexes ($E^{\#}$) of 14 kDa PLA2 (*4*) and phosphatidylinositol specific phospholipase C (*5*) are formed with monodisperse amphiphiles. Properties of $E^{\#}$ are likely to provide a better understanding of the interactions involved in interfacial binding and activation. For example, formation of the $E^{\#}$ complexes of PLA2 with alkyl sulfate is sensitive to certain single-site mutations located away from its i-face (*4*).

The i-face of an interfacial enzyme is designed to bind organized interfaces of amphiphiles. Therefore, it is not surprising that the i-face should also have a tendency to bind and organize monodisperse amphiphiles. As conceptualized in Figure 1 and developed in the Appendix, monodisperse amphiphiles could form premicellar $E_i^{\#}$ complexes. The equilibria between E, E*, and $E_i^{\#}$ are related by detailed balance conditions. In addition, the amphiphilic character of $E_i^{\#}$, due to the exposed alkyl chain, promotes self-aggregation of such complexes. Thus, $E_i^{\#}$ and micellar E* complexes,

† This research was supported by NIH Grant GM-29703 (M.K.J.) and The Swedish Research Council (O.G.B.).

* To whom correspondence should be addressed. (M.K.J.) Phone: 302-831-2968. Fax: 302-831-6335. E-mail: mkjain@udel.edu.

‡ Uppsala University Evolutionary Biology Center.

§ University of Delaware.

[1] Abbreviations: CMC, critical micellization concentration; C_nSO_4, *n*-alkyl-1-sulfate of chain length *n*; DC_nPC-ether, 1,2-dialkyl-*sn*-3-glycerophospho-methanol; DC_nPM-ether, 1,2-dialkyl-*sn*-3-glycerophospho-methanol; i-face, interface binding surface of an interfacial enzyme such as PLA2; itc, isothermal calorimetry; MJ33, 1-hexadecyl-3-(trifluoroethyl)-*rac*-glycero-2-phosphomethanol; PLA2, secreted 14 kDa type IB phospholipase A_2 from pig pancreas. Parameters for analysis (Table 1) are defined in the text and Appendix eq 1.

10.1021/bi0497650 CCC: $27.50
Published on Web 06/04/2004

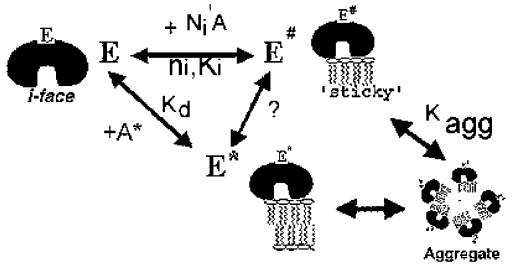

FIGURE 1: Paradigm for the interactions along the i-face of the enzyme. Binding of bilayer along the i-face of PLA2 forms only the E* complex without reorganization or disruption of vesicles. *E** on micelles reorganize the micelle and also form aggregates. Premicellar $E_i^{\#}$ complexes are formed by the binding of N_i' monodisperse amphiphiles along the i-face. On the basis of the model developed in the Appendix, results in this paper for PLA2 show that the binding of monodisperse amphiphiles to E to form the premicellar complex is a sequential three-step process (eq 1). Each step ($i = 1, 2, 3$) is cooperative with a Hill coefficient n_i and a dissociation constant K_i for the $E_i^{\#}$ complex. Properties of $E_i^{\#}$ suggest that that the complexes are readily reversible. The $E_i^{\#}$ complexes are also amphiphilic; with the polar group bound to the i-face, the alkyl chains are exposed to the aqueous phase. Therefore, as also modeled in the Appendix, $E_i^{\#}$ has a strong propensity to self-aggregate.

and their aggregates, have functional consequences. Such parallel and secondary processes (eq 12 in the Appendix) could not only interfere with the determination of the primary interfacial binding and related events but also have consequences for the activity of the enzyme with micelles or comicelles. First, the premicellar complexes will compete with enzyme binding to the micelles and thus influence the properties of a particular species. Second, the binding of monodisperse amphiphiles to the i-face could trigger allosteric interfacial activation of the enzyme in $E_i^{\#}$ and lead to apparent activity with monomeric substrates below the CMC (*4*). Furthermore, the plethora of binding states with micellar and premicellar amphiphiles will complicate the interpretation of all experiments involving the ligands that bind differentially to the i-face and the active site.

With an objective of identifying the primary events for the interfacial binding, here we report the quantitative analysis of the equilibrium interactions of monodisperse alkyl sulfates with the i-face of PLA2. Within the paradigm of Figure 1 as a heuristic guide, a three-step model (eq 1 developed in the Appendix)

$$\mathrm{E} \underset{n_1, K_1}{\overset{+N_1'A}{\rightleftharpoons}} \mathrm{E_1}^{\#} \underset{n_2, K_2}{\overset{+N_2'A}{\rightleftharpoons}} \mathrm{E_2}^{\#} \underset{n_3, K_3}{\overset{+N_3'A}{\rightleftharpoons}} \mathrm{E_3}^{\#} \qquad (1)$$

provides an analytical basis for the interpretation of the results. Equilibria for the sequential but stepwise binding of alkyl sulfate monomers to the i-face of PLA2 suggest that three discrete premicellar species are formed ($E_i^{\#}$, $i = 1$, 2, or 3). Possibly a different complex, E*, is formed with micelles of alkyl sulfate. A possible relationship between cooperative and stepwise amphiphile binding along the i-face and the allosteric activation of PLA2 by the anionic charge at the interface is suggested. Short-range specific interactions of the anionic headgroups with polarizable ligands on the i-face of PLA2 promote the hydrophobic effect and desolvation of the microinterface of the bound enzyme. Assumptions involved in the analysis and interpretation of the model, for the stepwise ligand substitution along the i-face to dehydrate the anionic headgroups of the cooperatively bound amphiphiles, are discussed. Since the E* and $E^{\#}$ species tend to aggregate, the analysis is also extended in the Appendix to describe the effect of such aggregation on the apparent characteristic parameters for the $E_i^{\#}$ complexes (eq 1) as are implicit in wide ranging results (*10*−*31*).

METHODS AND EXPERIMENTAL PROCEDURES

Amphiphiles were the of best grade (99%) available from Sigma, Aldrich, or Acros. Sources of other reagents, including the rationale for the choice of the experimental conditions and protocols for the CMC measurements, size exclusion chromatography, and the spectroscopic measurements are as established before (*4*−*10*). Specific conditions for the measurements are given in the text and figure legends. All measurements for the present study were carried out in 0.475 M NaCl, 20 mM Tris, 10 mM HEPES at pH 7 and 24 °C. These conditions are also optimal for the size-exclusion chromatography by HPLC (*4*, *5*).

UV Absorbance. Spectra were recorded at 23 °C on the diode array Hewlett-Packard UV−vis spectrophotometer (model HP8452) in a 1 cm path length cuvette in buffer containing 17 μM PLA2. Spectral manipulations were made with the software provided with the instrument. For the scattering correction, the intensity between 320 and 350 nm was used as the baseline to calculate the scattering contributions across the 240−320 nm range.

Fluorescence Changes. The tryptophan fluorescence emission spectra and the intensity changes from 2 μM PLA2 in 1.6 mL of stirred buffer in a 1 cm cuvette were measured on SLM-Aminco AB2. The slit-widths were 4 nm with excitation at 280 nm and emission at 333 nm.

Isothermal Calorimetric Titration. The enthalpy change on successive injections of alkyl sulfate to 1.412 mL of 17 μM PLA2 was measured with a Microcal (model VP-itc) calorimeter with a stirring speed of 300 rpm. Microcal (Origin) software was used for the integration of the incremental heat change. Control runs for amphiphile dilution were made without the enzyme. Except for the reactant concentrations, all other concentrations in the injection syringe and the reaction cell were identical. Such controls were necessary because the incremental heat change for the appropriate dilution of the amphiphile in the injection syringe was subtracted from the heat change measured in the presence of PLA2. For the fit to eq 4 (using the Origin or Mathcad software), the incremental heat changes were integrated to obtain the total heat change as a function of the total added amphiphile concentration in the cell.

Determination of CMC. The critical micellization concentration of amphiphiles was determined on a Roller−Smith surface tension balance (Du Nouy ring design) in 4 mL of 100 mM NaCl, 1 mM $CaCl_2$, and 10 mM Tris buffer at pH 8.0. Solutions were stirred after addition of each aliquot of lipid before measuring surface tension. The surface tension of the buffer (75 dyne) decreases with increasing amphiphile concentration and reaches a limiting value of about 30 dyn at the CMC. PLA2 alone does not noticeably change the surface tension; however, the concentration dependence for the long-chain amphiphiles with low CMC changes significantly in the presence of PLA2 in the subphase. This is expected if the premicellar complexes remain in the aqueous phase.

Table 1: Fit Parameters for the Binding of Alkyl Sulfate to PLA2[a]

amphiphile	+	χ^2	K_1	K_2	K_3	a_1	a_2	a_3	n_1	n_2	n_3	CMC
C_6SO_4	Ca	.01	4000	17 000	60 000	.06	.11	.04	2.3	6.8	4	80 000
C_8SO_4	Ca	.05	870	8800	36 000	.21	.25	.44	1.4	14.6	6.2	35 000
$C_{10}SO_3$	Ca	.04	700	2400		.26	.59		.93	6.1		4000
$C_{10}SO_4$	Ca	.04	70	750	4000	.26	.67	.59	2.1	8.3	12	4500
$C_{10}SO_4$	EGTA	0.02	80	800	4700	.19	.64	.61	2.6	5.7	10	4500
$C_{11}SO_4$	EGTA	0.06	90	180	680	0.19	0.87	0.82	1.1	5.9	6.1	800
$C_{12}SO_4$	Ca	.77	40	62	210	1.67	1.05	.57	2.4	6.1	5.8	200
$C_{12}SO_4$	EGTA	.28	18	40	160	.2	.85	.44	1.8	4.5	5.6	200
$C_{14}SO_4$	EGTA	.13	9	22	130	.18	.89	.46	1.7	3.7	3.1	50
DC_6PM-ether	Ca	.05	60	1860		.033	.08	-	2.7	10	-	3500
$\delta\Delta G_{CH_2}^{app}$			−0.46	−0.56	−0.55							−0.57

[a] Relative Trp-fluorescence increase of 2 μM PLA2 in 0.475 M NaCl, 20 mM Tris, and 10 mM HEPES at pH 7 and 24° C without or with 0.5 mM $CaCl_2$ was monitored at 333 nm. The fit parameters are for eq 4 (Appendix). χ^2 values are ×1000, i.e., 0.02 is 0.000002. The K_i and CMC values are in μM. The a_i values are expressed as $F/F_o - 1$. Statistical uncertainty in the fit parameters (fitted with the Origin software) is 20% for the first two steps and 50% for the third step.

Considerations for Solution Behaviors of Anionic Amphiphiles. The sub-CMC concentrations of amphiphiles provide the essential window of conditions needed to monitor the equilibrium binding of monodisperse amphiphiles (*4*, *5*). Irrespective of the method used to monitor the complex formation, the results are in quantitative accord with the model in eq 1. Additional considerations are given below. The CD and fluorescence changes indicative of denaturation of PLA2 are not observed in the presence of monodispersed alkyl sulfates, or at the onset of micellization; possible denaturation at the higher concentration of micellar C12- or C14-alkyl sulfates at >2 times the CMC cannot be ruled out. Calorimetry titrations require consideration also of other changes since the enthalpy change is the sum total of all contributions from the changes between the initial and the final states of all the species present in the reaction mixture. Furthermore, the problem of identifying the origin of modest enthalpy changes is compounded by the fact that the dilution, solubility, and the phase behaviors of ionic amphiphiles also depend on the pH and salt and calcium concentrations. The range of the apparent dissociation constant for calcium with alkyl sulfates is between 1 and 20 mM with a significant difference between the monodisperse and the (co)micellar amphiphiles. Also, modest heat changes can only be monitored at high enzyme concentrations. As developed in the Appendix (eq 5 and Figures 13 and 14), under such conditions, the observed binding curve can be significantly distorted due to the depletion of titrant amphiphile. These effects limit the range over which the observed heat changes can be quantitatively interpreted because secondary contributions cannot be entirely eliminated. Suitably designed controls can minimize and compensate for these effects only under certain conditions. In addition to the enthalpy changes associated with the dilution of micelles, certain amphiphiles such as decylsulfonate ($C_{10}SO_3$ in Table 1) also undergo a slow phase change. At room temperature, the latency can be hours and days. If not properly controlled, such factors introduce anomalies. Fortunately, none of these limitations applies to the itc titration results with decyl sulfate.

Particle Size by the Scattering Measurements. Dynamic light scattering measurements were done on a SynaPro 801 instrument from Protein Solutions, Inc., through the courtesy of Dr. Frank Lewandowski, who also carried out data analysis with the standard software available with the instrument. Zimm and Debye plots were obtained from the variable scattering angle instrument from Wyatt Technology Corp. equipped with a DAWN data processing system (Santa Barbara, CA). These measurements were carried out at the Surgery Department of The Metrohealth Medical Center, Cleveland, OH. High concentrations (>0.2 mM) of PLA2 were required for the determination of the particle size in the absence of phospholipids. Typically, the scattering measurements on the aggregates were carried out with 3−30 μM PLA2 and 30−1000 μM amphiphile in 1 mM $CaCl_2$ and 10 mM Tris at pH 8.0.

Apparent MW by Size-Exclusion. Controls and precautions for the use of the derivatized silica-based matrices of Protein-Pak 300SW (Waters) or TSK-Gel 4000SW column (BioRad) for HPLC have been described before (*4*, *5*). Elution times were measured on a Rainin instrument equipped serially with absorbance (set at 220 nm) and fluorescence (emission at 345 nm and excitation at 280 nm) detectors. Turbidity or scattering effects do not permit a comparison of the protein concentrations in the eluent and thus distort the protein peaks and elution volumes. Salt concentrations and pH of the elution buffer were optimized to eliminate complications from the anionic matrix of 4000SW. The column was equilibrated with 50 mM phosphate buffer containing 0.5 mM $CaCl_2$ at pH 7, and the same buffer was used for elution. Since the amphiphiles used in this study are anionic, we believe ion exchange does not contribute to the retention times of $E_i^{\#}$ and E* complexes during the molecular sieving. The separation range of the 4000SW column is 10 to 10 000 kDa. The molecular weights of the complexes were estimated from the calibration curve obtained with blue dextran (2000 kDa), ferritin (440 kDa), aldolase (158 kDa), bovine serum albumin (66 kDa), lactoglobulin (18.4 kDa), PLA2 (13.9 kDa), and cytochrome *c* (12.4 kDa). Since the elution times were determined with an accuracy of 0.1 min, uncertainty in the apparent molecular weights is about 20%. Between runs, the 4000SW matrix was regenerated by equilibrating the column with 0.5−1 M NaCl without flow, followed by wash with 15−20 column volumes of the elution buffer. Regeneration with 50% ethanol in water gave essentially identical results and is preferable for the stainless steel columns.

RESULTS

Effect of Decyl Sulfate on the Trp-Emission from PLA2. PLA2 has only one tryptophan (Trp-3), which is localized

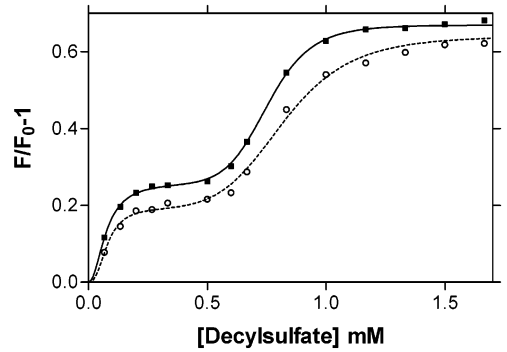

FIGURE 2: Increase in the tryptophan fluorescence emission intensity at 333 nm (excitation at 280 nm) from 2 μM PLA2 in (circle) EGTA or (squares) 0.5 mM calcium as a function of decyl sulfate concentration. The lines are for the nine-parameter (Table 1) fit for the complete set of data (Figure 3) to eq 4.

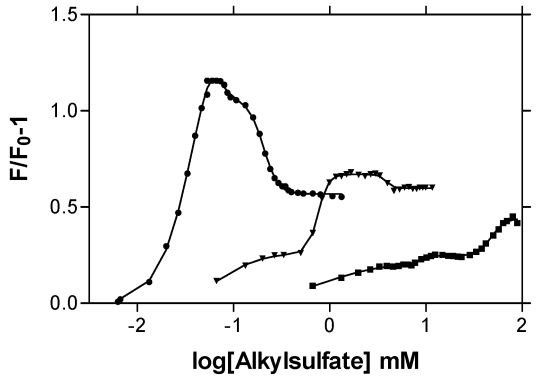

FIGURE 3: Change in the relative emission intensity (at 333 nm) of 2 μM PLA2 in 0.5 mM $CaCl_2$ as a function of amphiphile concentration (logarithmic scale). Results (from left) for dodecyl sulfate, decyl sulfate, and octyl sulfate. In each case, the continuous line is the fit to eq 4 with the fit parameters summarized in Table 1.

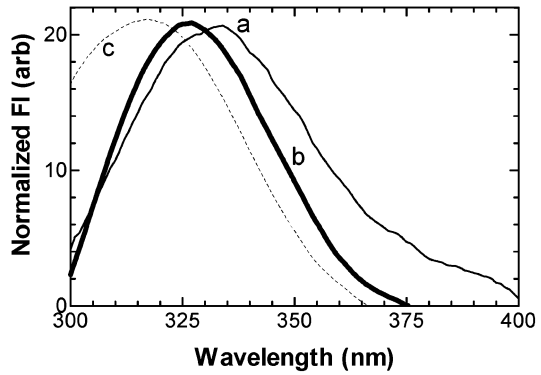

FIGURE 4: Normalized (to the peak) change in the fluorescence emission spectrum (excitation 280 nm) of 2 μM PLA2 in 0.5 mM $CaCl_2$ induced by (a) 0.3 mM, (b) 2 mM, and (c) 9.9 mM decyl sulfate. Similar but not identical changes were also obtained in the absence of calcium in the EGTA buffer. It is not unlikely that at 9.9 mM decyl sulfate there is a contribution from denaturation and the scattering change.

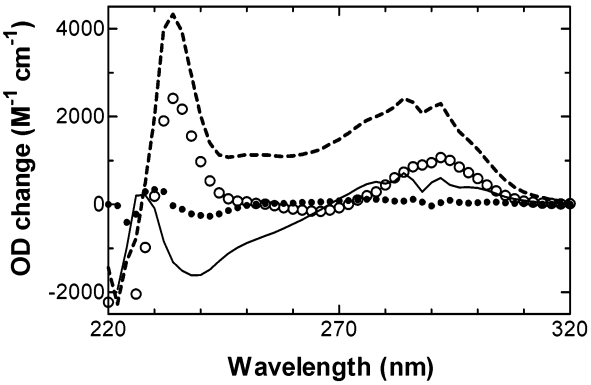

FIGURE 5: Decyl sulfate (for $E_2^{\#}$ at 1.48 mM with the lines and for $E_1^{\#}$ at 0.28 mM with the symbols) induced change in the UV absorbance spectrum of 17 μM PLA2 in the standard buffer with (continuous line or filled circles) 0.5 mM calcium or with (dashed line or unfilled circles) 1 mM EGTA + 1 mM EDTA. The difference spectra were obtained by subtracting the absorbance spectra corrected for the scattering.

on the i-face (*3*, *11*). Results summarized in Figures 2 and 3 reveal that the fluorescence emission intensity of Trp-3 is influenced by decyl sulfate binding in each of the three steps (eq 1) as well as on the binding of PLA2 to micelles. Below the CMC, summarized in the last column of Table 1, at least two steps are clearly discernible (Figure 2), and a third step is seen near the CMC (Figure 3). The fluorescence emission difference spectra in Figure 4 show characteristic changes for the $E_1^{\#}$, $E_2^{\#}$, or E* complex in the presence of decyl sulfate relative to the free PLA2 (E form). Results not shown here reveal that comparable, but not identical, changes are seen in the presence of added calcium or EGTA. Successive addition, dilution, and mixing manipulations with $E^{\#}$ and E* and their aggregates suggest that these complexes are reversible and reequilibrate on the time scale of few seconds. Together, these results show that formation of different $E_i^{\#}$ complexes is associated with a distinct change in the tryptophan environment in PLA2. A significant increase in the intensity at 300 nm is seen at the micellar concentrations where PLA2 may be denatured.

Decyl sulfate-induced perturbation of tryptophan in $E_1^{\#}$ and $E_2^{\#}$ in the presence or absence of calcium is clearly apparent in the changes in the absorbance spectrum (Figure 5). Changes in the absorbance observed at 292, 295, and 305 nm are consistent with the possibility that the polarity, solvent accessibility, and H-bonding to Trp-3 change in the $E_i^{\#}$ complexes. The change at 284 nm could involve tyrosine, whereas the changes in the 235 nm region could be due to changes in histidine and tyrosine environments (*12*). UV-spectral changes also show a dependence on the alkyl sulfate concentration corresponding to the formation of $E_1^{\#}$ and $E_2^{\#}$, and the fit parameters for the formation of $E_1^{\#}$ are comparable to those obtained from the fluorescence change (Table 1). Significant turbidity changes associated with the formation of $E_2^{\#}$ and $E_3^{\#}$ precluded the analysis of the OD changes. Such effects are not significant for the fluorescence change (Figures 2 and 3) because the magnitude of the turbidity changes is intrinsically larger than the 90° scattering changes. As described further below, alkyl sulfate-induced changes are also observed by isothermal calorimetry, size-exclusion chromatography, and the laser light scattering measurements.

Model for the Three Consecutive Hill Steps. Analysis and interpretation of the binding isotherm based on the fluorescence change (Figures 2 and 3) is based on the assumption that the three complexes are sequentially formed in the presence of monodisperse alkyl sulfate (Appendix). The nine fit parameters for the three steps of the Trp-emission changes in the presence of the alkyl sulfate homologues are summarized in Table 1. These results show that the chain length

of alkyl sulfate has a significant and systematic effect on the values of the fit parameters. While the range for the dissociation constants (K_i) is about 1000-fold, the Hill coefficients (n_i) for each of the steps remain relatively unchanged. The K_i and n_i values are at best marginally different in the presence of calcium, the catalytic cofactor that is also required for the binding of the active-site-directed ligands (*9*). In the presence of EGTA, the alkyl chain length has the biggest effect on K_2, while in the presence of Ca^{2+}, chain length affects both K_2 and K_3. The magnitude of the fluorescence increase a_2 for the formation of $E_2^{\#}$ from E, as well as the value of a_3 for the E to $E_3^{\#}$ change, increases with the chain length, as also seen for the intensity of an energy transfer probe (*4*).

Specific models consistent with the paradigm for the interaction of amphiphiles along the i-face (Figure 1) are developed in the Appendix. If we are to think of the i-face of PLA2 as consisting of sets of different binding sites, the binding can be modeled in many different ways. Analysis of the sequential binding of amphiphiles to the successively formed $E_i^{\#}$ complexes (eq 1) is based on a tacit assumption that each binding event creates the site where the next set of amphiphiles can bind to form the next complex. Thus, cooperativity would involve contributions from the interactions of the amphiphiles along the i-face and also from the hydrophobic propensity of amphiphiles binding next to each other. As described, the observed cooperativity is interpreted in terms of an all-or-nothing (Hill) binding of a certain number of amphiphiles to some specified region of the enzyme.

We believe that the sequential scheme (eq 1) adopted here is a minimum model. However, other cooperative binding models, which we have not considered here, can give similar results but would require different interpretations of the estimated parameter values. As developed in the Appendix, eq 4 is meaningfully applied as the minimum model if the three steps can be clearly distinguished in the data, as is the case for the results analyzed in this paper. Our reliance on this model comes from the discrete stepwise changes in the tryptophan emission intensity as a function of the amphiphile concentration (Figures 2 and 3). Reliable and unique fits to all parts of a binding isotherm can be expected only if the steps are sufficiently separated. Note that eq 4 can be readily adopted for two- or one-step models where a satisfactory fit could mean that additional steps may not be there or are not distinguishable in the results. Statistical uncertainty in the parameter values is not given here. However, on the basis of the standard deviation, uncertainty in the parameter values for $E_1^{\#}$ and $E_2^{\#}$ is 20% and about 50% for $E_3^{\#}$. Note that the χ^2 values for the fits in Table 1 are from 10^{-3} to 10^{-6}. Scatter is hardly noticeable at this level of fit.

With all multiparameter fits there is always some cross-variation between the parameters. To some extent the covariance values meaningfully distinguish and evaluate the goodness of fit with multiple floating parameters. Many of the standard programs (such as Origin) give covariance between the fit parameters along with a measure for the goodness of the fit (standard deviation and χ^2). Attention to such details gives an appreciation of the range over which the fit parameters can be meaningfully distinguished. The possibility of being stuck in a local minimum can be avoided by starting with good initial guesses and also by keeping a visual track of the fit during iterations for the fit. Note that different fitting programs may focus on different parts and quirks of the curves that the program decides to adjust to. Such quirks become apparent when comparisons are made between the data sets where systematic incremental changes are expected.

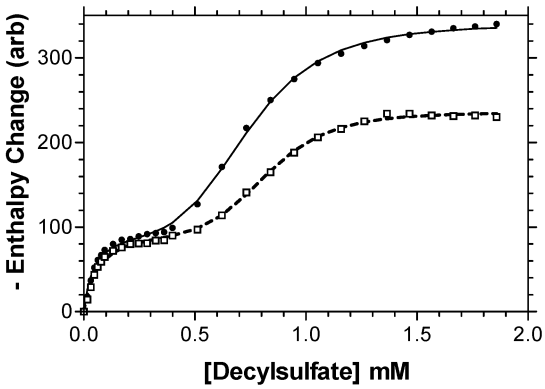

FIGURE 6: Net heat change (exothermic in arbitrary units) as a function of decyl sulfate (11.1 mM in the injection syringe) successively added to 1.421 mL of balanced standard buffer containing 17 μM pig PLA2 with (unfilled square) 1 mM EGTA and 1 mM EDTA or (filled circle) 0.5 mM calcium. Heat of dilution of decyl sulfate in the calcium buffer without PLA2 is subtracted from the results (not shown). The fit (continuous line) parameters to eq 1 for both curves are $K_1 = 80$ μM with $n_1 = 1.4$ and $K_2 = 700$ μM with $n_2 = 8$. The total enthalpy change is -10 kcal/mol PLA2 in EGTA and -15 kcal/mol PLA2 in the presence of calcium.

Enthalpy Change on Titration of PLA2 with Decyl Sulfate. As shown in Figure 6, an exothermic enthalpy change occurs during isothermal titration of 17 μM PLA2 with decyl sulfate. Below 2 mM, the net change in the enthalpy (corrected for the dilution of decyl sulfate) is biphasic. The fit parameters (given in the legend to Figure 6) suggest that the formation of $E_1^{\#}$ and $E_2^{\#}$ is exothermic, and the enthalpy change for the second step is significantly higher in the presence of calcium. These fits were carried out assuming that there is no significant depletion of decyl sulfate during the titration, i.e., the total concentration is approximately equal to the free decyl sulfate concentration. Simulations shown in Figure 13 support this assumption. These simulations are based on the assumed values for the decyl sulfate stoichiometry per PLA2 for $E_1^{\#}$ as N_1 and for $E_2^{\#}$ as N_2. Note that the depletion is not likely to be noticeable with $N_1 < 10$ and $N_2 < 30$ with the other parameter values obtained below 20 μM PLA2 as in Figure 6 or Table 1. Other simulations in Figures 13 and 14 demonstrate that increasingly significant contributions of the depletion from the complex formation are expected above 20 μM PLA2. The simulations further suggest that even at 2 μM PLA2 depletion could be significant enough to slightly distort the parameter values for dodecyl sulfate, and certainly so for tetradecyl sulfate (Table 1).

The primary effect of neglecting the depletion will be distortion of the binding curves, making the cooperativity, n_i, appear to be smaller and the dissociation constant, K_i, appear to be larger. For reasons developed in the Appendix (eq 5), the stoichiometry factors, N_1, N_2, and N_3, cannot easily be determined from the measurements at hand unless some parameters are known from other results. Results described below indicated that the $E_i^{\#}$ species tend to aggregate. As expected, the aggregation tendency increases at the higher decyl sulfate as well as PLA2 concentrations. On the basis

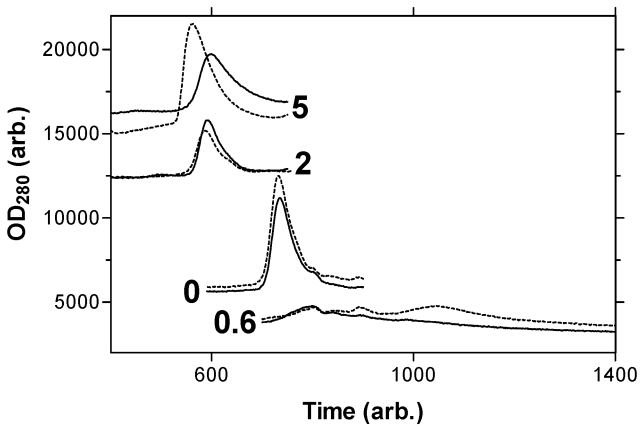

FIGURE 7: Elution profiles (at 1 mL/min flow rate) for 10 μg of PLA2 from the size-exclusion column (Protein-Pak 300SW from Waters) equilibrated with buffer containing (dashed line) 1 mM EGTA + 1 mM EDTA or (continuous line) 0.5 mM calcium with (as indicated) 0, 0.6, 2, or 5 mM decyl sulfate. For clarity, the profiles are vertically shifted, and both scales are arbitrary but constant for all runs.

of the results and analysis presented thus far, it also appears to be possible that the $E_i^{\#}$ complexes could bind additional amphiphiles ("growing complex") even after the fluorescence signal is saturated. Such effects precluded attempts to determine values of N_1 and N_2. However, results described below provide clear evidence that large aggregates of PLA2 indicative of premicellar $E_i^{\#}$ formation are formed in the presence of structurally diverse monodispersed anionic amphiphiles.

Size-Exclusion Behavior of PLA2 in the Presence of Decyl Sulfate. The behavior of PLA2 on size-exclusion column equilibrated with alkyl sulfate shows complex amphiphile concentration dependence (*4*, *5*). As summarized in Figure 7, the effect of decyl sulfate concentration on the elution profile for PLA2 is dramatic and complex, yet the results are qualitatively consistent with the model in eq 1 and Figure 1. The experimental conditions used to generate the results in Figure 7 are such that, according to the parameters in Table 1, virtually all PLA2 is present in the E form at 0 mM decyl sulfate, as $E_1^{\#}$ at 0.6 mM, as $E_2^{\#}$ at 2 mM, and as $E_3^{\#}$ (or E*) at 5 mM decyl sulfate. The longer retention time at 0.6 mM decyl sulfate suggests that $E_1^{\#}$ "sticks" to the Protein-Pak matrix. The $E_2^{\#}$ form at 2 mM decyl sulfate elutes as an aggregate of apparent molecular weight 120 kDa. In the presence of calcium, the aggregate sizes for $E_2^{\#}$ and $E_3^{\#}$ are comparable; the size of the $E_3^{\#}$ aggregate increases noticeably in EDTA. These apparent size estimates are based on the assumption that the size-exclusion behavior of the aggregate is comparable to that of the globular proteins used as the calibration standards.

Aggregates with Substrate Analogues. Size estimates from the light-scattering behaviors of PLA2 in the presence of different substrate analogues are summarized in Table 2. In all cases, large aggregates are formed even below the CMC. Particularly interesting are the Zimm plots in Figure 8 obtained at several concentrations of the aggregate from the scattering intensities at 15−165° relative to the incident light. A good first order fit is expected for a small molecule like PLA2 (Figure 8A). In fact, extrapolation to zero protein concentration gives an estimated molecular weight of 13−16 kDa, in good agreement with the monomer molecular weight of 14 kDa. The angular dependence of the scattered intensities from PLA2 is ideal over a broad concentration range. These results show that in the absence of amphiphile, PLA2 is monomeric. Also, both PLA2 and its catalytically inert zymogen proPLA2 show little, if any, tendency to form oligomers up to 200 μM concentrations in the aqueous phase.

Table 2: Size Estimates for the PLA2 Aggregates (MW in kDa)[a]

PLA2/conditions	Zimm plot	QLS	size exclusion
<0.4 mM PLA2	13.6 ± 0.7	17 ± 2	14 ± 3
+ DC_6PM-ether	2000	>1000	
+ DC_8PM-ether	>500	>1000	>1000
+ $C_{16}SO_4$	>500	>1000	
+ $C_{12}SO_4$	>1000		
+ DC_8PC-ether	15	16	15
+ MJ33 + DC_8PC-ether	320	>1000	>1000
Pro-PLA + MJ33 + DC_8PC	15		

[a] These measurements were carried out in 10 mM Tris at pH 8.0 and 23 °C. The CMC values were 0.02 mM for DC_8PC-ether and 0.03 mM for DC_8PM-ether; for other values, see Table 1. Uncertainty in the particle sizes obtained by these methods is estimated to be less than 30%. QLS, quasielastic light scattering.

The Zimm plot in Figure 8B, for a mixture of 12 μM PLA2 with 12 μM MJ33 and 0.4 mM DC_8PC-ether, shows that the apparent molecular weight of the aggregate is about 300 kDa. The apparent particle size does not change with changing the bulk concentration of both components at a constant ratio. The second- and third-order fits (not shown) are as expected for large particles with broad dispersity. This is also consistent with results in Figures 9 and 10 and Table 2. Fore example, particles formed in the presence of monodisperse DC_6PM-ether apparently contain 10−15 PLA2 monomers, perhaps some kind of self-packing limit. Similar studies with DC_8PM and the longer chain alkyl sulfates suggest that the aggregate size is very large. Note that under comparable conditions, the aggregate is not formed with proPLA2 (Table 2).

Dynamic light scattering measurements confirm that in 0.4 mM solution, PLA2 is present (for the 95% of intensity) as a monomer of hydrodynamic radius of 2 nm corresponding to a molecular weight of 14 kDa (Table 2). A propensity to form oligomers is indicated at higher salt concentrations in the presence of certain buffers, but we did not characterize such oligomers. Considerably larger aggregates are formed in the presence of monodisperse DC_8PM-ether or DC_6PM-ether. Fits of the scattered intensity data to appropriate models indicated that possibly two aggregated species are formed. As summarized in Figure 9, the relative proportion of the two complexes, rather than their size, changes with the phospholipid/protein ratio. At low DC_6PM-ether concentrations, a high molecular weight species dominates, whose molecular weight is estimated to be more than one million. At higher concentrations of DC_6PM-ether, the proportion of the lower molecular weight species increases. Its molecular weight is estimated to be about 300 kDa with a hydrodynamic radius of 35 nm. These results further show that PLA2 and DC_6PM-ether or DC_8PM-ether form aggregates. Their size and dispersity remain to be established.

As shown in Figure 10, PLA2 aggregates with DC_8PM-ether elute as large molecular weight species on size-exclusion chromatography through an unequilibrated column. A mixture of PLA2 and DC_8PM-ether, presumably in the E* form, was applied to the column equilibrated with only

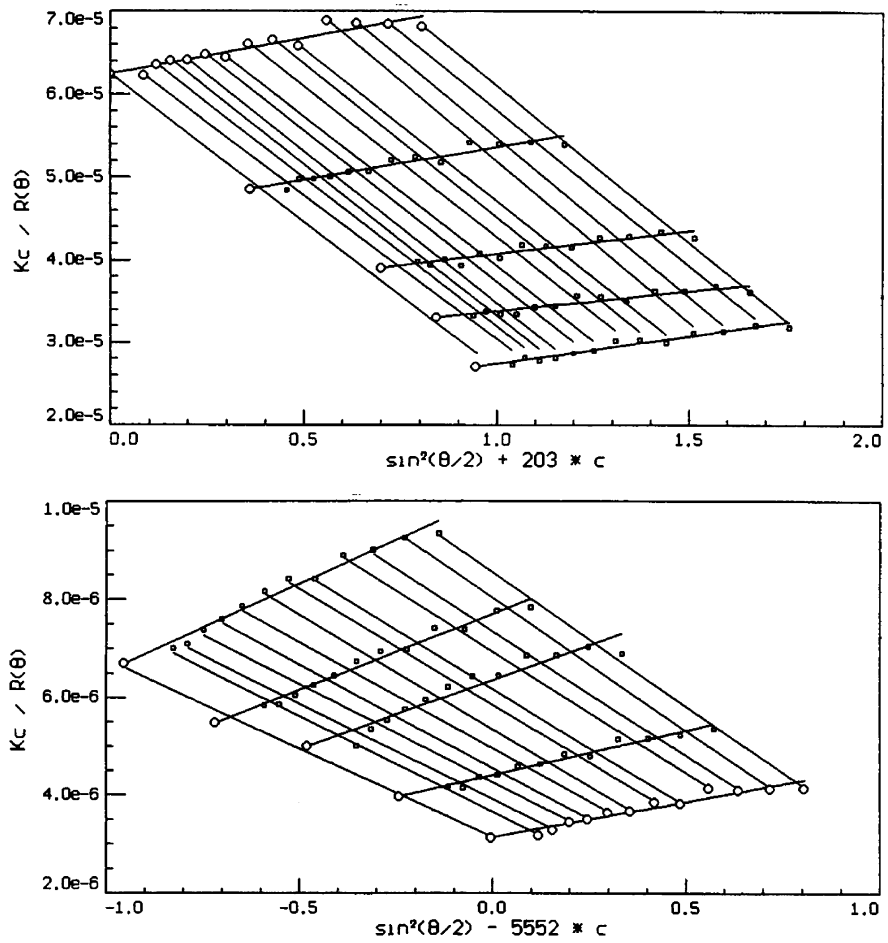

FIGURE 8: First-order Zimm plots for scattered light intensity from [A, top] PLA2 alone or [B, bottom] a mixture of PLA2 with DC_8PC-ether and MJ33 (1:30:1 mole ratio). The molecular weight, the reciprocal of the common intercept, in A is 14 kDa with a RMS radius of 24 nm, while that in B is 320 kDa with a RMS radius of 45 nm. These measurements were carried out in 1 mM $CaCl_2$ and 10 mM Tris·HCl buffer at pH 8.0 and 23 °C.

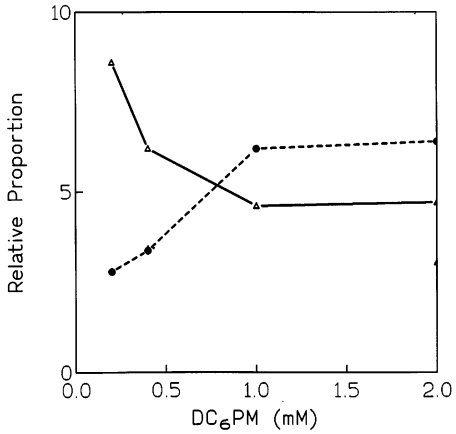

FIGURE 9: Changes in the relative amounts (arbitrary scales) of the larger (unfilled triangle) and smaller (circles) particles as calculated from the dynamic light scattering measurements with 0.2 mM PLA2 (2.2 nm radius) and increasing concentration of DC_6-PM-ether (CMC = 4.5 mM).

the phosphate buffer. PLA2 alone elutes at 11 min (peak), and the elution profile for the aggregates suggests anomalous retention (*4*, *5*). At low lipid/enzyme ratio PLA2 elutes in a peak at 4.35 min, near the void volume (3.9 min). This is expected if the aggregate size is near 1000 kDa. The peak width suggests partial dissociation of the complex. At the highest lipid/PLA2 ratio, the enzyme elutes in two peaks corresponding to molecular weights of 1000 and 350 kDa. On changing the lipid/PLA2 ratio from 30 to 800, the proportion of the smaller MW species increases at the expense of the larger aggregate (results are not shown but are consistent with results in Figure 9). Together, the results in Figures 7−10 and in Table 2 show that in the presence of monodisperse and micellar amphiphiles, large aggregates are formed by PLA2, with or without occupancy of the active site. Our attempts to obtain information about the size dispersity and equilibrium behaviors of the complexe(s) were not successful.

DISCUSSION

Separate identity of the catalytic site and the i-face is critical for the conceptualization of the function and structure of interfacial enzymes (*1*−*3*, *11*, *21*). A single vesicle-bound E* species carries out the steps of the processive interfacial turnover by PLA2 on dimyristoylphosphatidyl-methanol vesicles (*22*−*24*). Thus, a fully functional monomeric E* species suggests that the lipid interactions with a monodisperse PLA2 are sufficient for the catalytic turnover and its allosteric regulation. Also the substrate exchange rate in the complexes (and aggregates?) of PLA2 with the short chain phosphatidyl-methanol is rapid ,and the chemical step remains rate-limiting even at the turnover rates above 1000 s^{-1} (*10*, *17*−*19*). Kinetic results also show that PLA2 is not denatured by monomers or micelles of the short-chain

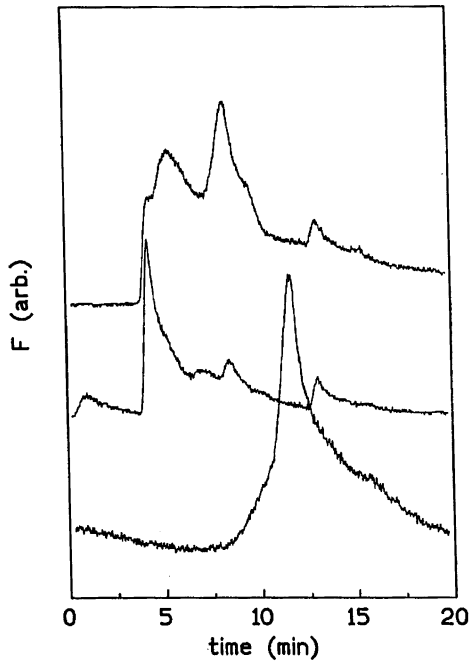

FIGURE 10: HPLC elution profiles from TSK 400SW size-exclusion column (from bottom) of 16 μg of PLA2 (1.12 nmole) alone or with 1:50 or 1:400 (top) mole ratio with DC_8PM-ether. Elution was monitored as fluorescence emission. Under these conditions, the lipid alone did not show any signal. Hydrophobic interactions of PLA2 with the column matrix gives rise to the elution profile (4, 5). Note that here the column is not preequilibrated with the amphiphile, whereas results in Figure 7 are for the equilibrated column.

zwitterionic or anionic phospholipids. Since aggregates are formed under these conditions, we conclude that aggregation as such does not have an effect on the turnover or its allosteric K_S* and k_{cat}* regulation. Altogether, tight binding of PLA2 to anionic vesicles is the basis for the processive interfacial catalytic turnover (*1*, *2*, *22*, *23*), and compensation of the cationic charge of K53, K56, and K120 is responsible for the allosteric k_{cat}* activation (*10*, *25*, *26*). We believe that the control of interfacial allostery (*1*, *2*, *4*, *25*, *26*) is modulated through specific interactions of amphiphiles with the i-face of the enzyme at the interface.

As shown for the PLA2 mutants (*4*), phosphatidyl-inositol-specific phospholipase C (*5*), and sphingomyelinase (in preparation), as a part of paradigm in Figure 1, formation of the premicellar $E_i^{\#}$ complexes with monodisperse amphiphiles is likely to be a general property of the interactions along the i-face (interfacial binding surface) of interfacial enzymes. Aggregation of the E* and $E_i^{\#}$ complexes raises issues not only about the nature of the additional protein−lipid and protein−protein interactions but also about the functional significance of the aggregate formation. It calls into question the interpretation and significance of all measurements with interfacial enzymes in the presence of monodisperse and micellar amphiphiles.

Results with secreted PLA2 show that premicellar aggregates are formed under wide-ranging conditions (*4*, *10*, *13*−*20*, *27*−*30*). Such effects can have their origins in distinctly different elemental steps within the interfacial binding paradigm. As outlined below, the consequences, and possibly the functional significance, of comicellization and aggregate formation are far reaching: Although aggregation may have its origins in steps that are distinctly different from those of the interfacial turnover path, it could still influence the parallel kinetic and equilibrium processes. Results with monodisperse amphiphiles and PLA2 show that at the very least, anomalous effects of the aggregate formation have to be ruled out.

(a) Anomalous substrate concentration dependence has been reported with diacyl-glycero-3-sulfate (*15*, *16*) as if the substrate replenishment rate is influenced by the aggregate formation. Similarly, in the mixed-micelles, the substrate replenishment rate becomes rate-limiting (*31*). Here the kinetic concern is primarily about the rate of substrate replenishment, and not about the rate of exchange of the codispersed detergent.

(b) Models developed in the Appendix clearly show that the equilibrium measurements with premicellar $E_i^{\#}$ and its aggregates would provide an average measure of the signal from all the $E_i^{\#}$, E*, and the aggregates. If, for example, the affinity of an active-site-directed ligand is monitored, the results will be skewed toward the bound form of the enzyme, which is K_S*-activated (*10*, *18*, *32*). This is because the affinity for the active-site-directed ligand is 20−100-fold higher for the E* form of pig pancreatic PLA2 than it is for the E form (*33*). On the other hand, the spectroscopic measurements will show a broader distribution of the signals that arise from the $E_i^{\#}$ and E* forms (*34*, *35*). Amplitudes of such signals depend on the nature of the amphiphile and may also be influenced by aggregation.

(c) Zwitterionic phospholipids emulsified with bile acids are the physiological substrates for the pancreatic PLA2 (*21*), which is consistent with the preference of pancreatic PLA2 for the anionic interface, which may or may not be related to specific binding of anionic amphiphiles to the i-face. Therefore, an understanding of the catalytic properties of the complexes and the underlying equilibria is crucial for the evaluation of the catalytic significance of the complexes that may coexist in the bile salt dispersed physiological substrate of PLA2. Similar selectivity, but not necessarily for the anionic amphiphiles, is also apparent for other interfacial enzymes, including the PLA2 isologues (*4*, *5*, *27*−*30*).

(d) On the basis of the detailed balance conditions (*34*), it is reasonable to assume that the affinity of the i-face for the monodisperse amphiphiles could be different depending on whether the active site is occupied or not. Therefore, for the measurements in the presence of two or more amphiphiles, one should consider the K_S* allostery, as well as the possibility of comicellization with a considerably lower intermicellar concentration.

Possibilities within the interfacial binding paradigm (Figure 1 and Appendix) suggest that the consequences of the coexistence of structurally diverse species such as $E_i^{\#}$, E*, and their aggregates in equilibrium with the E form are far-reaching. However, results at hand suggest that protein−protein interactions in such species are not likely to have any functional significance.

Anion Binding Along the i-Face. As discussed below the alkyl sulfate binding parameters (Table 1) obtained under suitably constrained conditions provide insight into the atomic-level short-range interactions along the i-face that stabilize the $E_i^{\#}$ complexes of PLA2. A structural model of the i-face of PLA2 (*11*) is in excellent accord with the crystal structure of the anion-assisted homodimer of IB PLA2 (*30*−

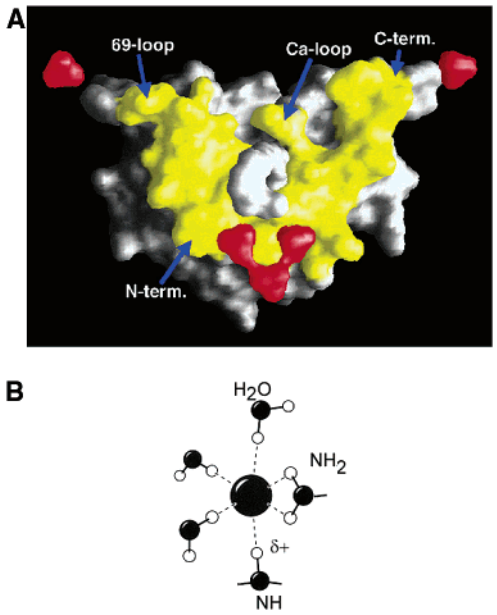

FIGURE 11: [A] i-Face of PLA2 displayed with the five bound sulfate anions shown in red (see *10*, *26*−*28* for details). The cluster of three sites (lower middle) is near the N-terminus with Trp-3. Residues of PLA2 that contribute ligands (Figure 11B) for the cluster of anions are Arg-6, Leu-19, Met-20, Lys-10, and several water molecules; NH of Glu-40 is the ligand for the second anion (upper left), and the side-chain carbonyl of Asn-112 is the ligand for the binding of the third anion (upper right). So far, the bound anions have been found only in the dimers. The active-site-directed ligand (white) protrudes from the middle. The desolvated hydrophobic surface (shown in yellow) could make close contact with the interface. As discussed in the text, cooperative binding of anionic amphiphiles could successively lead to the formation of $E_1^{\#}$, $E_2^{\#}$, and $E_3^{\#}$ (reproduced from *26*). [B] Ligands NH_2 or NH (smaller filled circles) with polarized hydrogen (unfilled circles with δ+) that substitute the polarized hydrogens of the hydrated water molecules bound to an anionic (large filled circle) atom such as the oxygen of sulfate, phosphate, or carboxylate. For such short-range interactions, the distance between the heavy atoms is 2.7−3 Å. Note that the partial cationic charge on the hydrogen atoms (without a net charge on the ligand) compensates the opposing charge on the anion.

32). As shown in Figure 11A, five anions bound to the protein ligands bring the desolvated i-faces of the two PLA2 molecules with occupied active site into close contact within about 4 Å. The hydrophobic effect comes into play as a result of the short-range specific anion binding as the water molecules bound to the anions are substituted by the polarized hydrogens of the amide, imino, and amino N−H (Figure 11B) on the i-face of PLA2.

Trp-3 as the Common Locus. The fluorescence signals a_i in Table 1 originate from Trp-3 on the i-face (Figure 11A). It is the only tryptophan in PLA2 (*11*). Since it is unlikely that a single amphiphile binding site is involved in all three steps (Figures 2 and 3), Trp-3 must be differentially perturbed by the successive amphiphile binding along the three different regions on the i-face of PLA2. As also indicated by the absorbance changes (Figure 5), the a_i values could reflect an alteration in the relationship of Trp-3 to its neighboring internal quencher groups, the solvent water, and the polarity of the microenvironment. On the basis of the position of Trp-3 on the i-face, we suggest that the first complex $E_1^{\#}$ is formed by the binding of three anionic amphiphiles to the cluster of three anion binding sites near the N-terminus. $E_2^{\#}$ would be formed next with the occupancy of one of the other two single-anion binding sites. A cooperative binding of $\geq n_2$ amphiphiles along their headgroups could fill the gap between the first and second sites. Formation of $E_3^{\#}$ as a fully developed premicellar complex would occur as the remaining anion binding site is occupied and the intervening gap is filled by the cooperative binding of $\geq n_3$ amphiphiles. At this stage, we cannot even speculate on the nature of the difference between $E_3^{\#}$ and E* (however, see below).

Model for the Binding of Anionic Amphiphiles. The fit parameters in Table 1 are for cooperative amphiphile binding in three steps (eq 1). Each of the complexes is characterized by a dissociation constant (K_i), Hill coefficient (n_i), and saturable maximum signal (a_i). Note that the binding parameters are only modestly influenced by an absence of calcium (Table 1), an obligatory cofactor for the binding of active-site-directed ligands to PLA2 as well as for the chemical step (*9*, *12*, *37*, *38*). Therefore, the E and E·Ca forms bind with virtually the same affinity to the preformed interfaces, and the amphiphile binding affinity in $E_i^{\#}$ and $E_i^{\#}$Ca is not significantly different either. These results imply that calcium does not promote the binding of alkyl sulfate to the active site of PLA2.

Sequential or Parallel Steps. Strictly speaking, the sequential model in eq 1 cannot be mathematically distinguished from a model in which the cooperative binding in the second step is independent of the binding in the first step. In either model, detailed balance relations apply to all equilibria. It is convenient to use the sequential model because the steps that can be identified experimentally involve the same Trp-3 and occur sequentially one after the other (Table 1, Figures 2, 3, 5, and 6). More crucial is the assumption that each step can be described as a Hill (all or nothing) binding process, where n_i amphiphiles bind simultaneously to form $E_i^{\#}$. If the cooperativity in each step is less than total, the estimated Hill parameter (n_i) would be smaller than the real number of amphiphiles involved (N_i'). Similarly, the estimated dissociation constant (K_i) would correspond to some average for these amphiphiles that bind in the cooperative step. In this way, K_i is expected to carry information about the average strength of interaction even if the cooperativity is not total.

Dissociation Constants. It is significant that all the K_i values for the homologous amphiphiles are nearly proportional to CMC (Table 1, Figure 12), i.e., the differences in the K values that we find are consistent with differences in their hydrophobic drive as manifested in their CMC. It suggests that the difference in the propensity to form $E_i^{\#}$ complex with monodisperse amphiphile is driven by the same difference in hydrophobic drive as micellization.

Since all three equilibria are cooperative and described only by apparent parameters, a proper thermodynamic analysis of the free energy and enthalpy of the amphiphile binding is not possible. The estimated values of K_i are model-dependent and do not necessarily correspond to any "real" dissociation constants. They are apparent equilibrium constants fitted to a Hill equation. Thus, the Hill constants K_1, K_2, and K_3 cannot be used to infer the absolute interaction free energy. We could describe the cooperative binding with other models and equations that would fit equally well but give different equilibrium constants (and different free energies). The dissociation constants are operationally defined such that 50% binding occurs at the concentrations K_1,

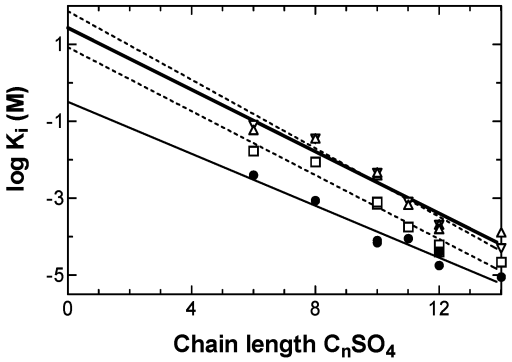

FIGURE 12: Plot of the dissociation constants (K_i on the log scale) as a function of the alkyl chain length: (circle and fine line) K_1, slope −0.34, *y*-intercept −0.49 (r^2 0.95); (square and dotted line) K_2, slope −0.42, *y*-intercept +0.93 (r^2 0.95); (triangle and thick line) K_3, slope −0.40, *y*-intercept +1.44 (r^2, 0.92); (inverted triangle and dashed line) CMC, slope −0.46, *y*-intercept +1.86 (r^2, 0.96). Values for tetradecyl sulfate are only the upper limit estimates due to the contributions from enzyme depletion (eq 5). Note that at room temperature, 1.36 x slope is $\delta\Delta G_{CH_2}^{app}$ (Table 1).

K_2, and K_3 (eq 2). Or more explicitly: $[E_1^{\#}]/[E] = 1$ at $c = K_1$; $[E_2^{\#}]/[E_1^{\#}] = 1$ at $c = K_2$; $[E_3^{\#}]/[E_2^{\#}] = 1$ at $c = K_3$. Since the dissociation constants clearly tell us about the strength of binding, though not the exact binding-free-energy, we can nonetheless discuss trends in the binding strength.

The dissociation constants for each of the three steps as well as the CMC values decrease with increasing chain length of alkyl sulfate (Figure 12). The trend holds even if the interpretation of the dissociation constants to obtain the equilibrium free energy is not entirely appropriate. The incremental free energy values per added CH_2, obtained from these plots as $\delta\Delta G_{CH_2}^{app}$ in the last row of Table 1, are in the range of about 0.5 kcal/mol. The magnitude of $\delta\Delta G_{CH_2}^{app}$ is a measure of the hydrophobic drive of each added CH_2 for the formation of the complex. The general trends (Figure 12) seem to be reasonable and significant and are consistent with the cooperative binding of the amphiphile driven substantially by the hydrophobic effect. The incremental free energy is presumably a measure of the extent to which the chains are shielded from water in the complexes (*39*−*41*).

The *y*-intercepts in Figure 12 correspond to the cratic contribution and to headgroup interactions. The unfavorable contributions in micelles without enzyme originate from headgroup to headgroup repulsions, and favorable contributions are expected from headgroup to enzyme interactions. The *y*-intercepts in Figure 12 are in the order CMC > K_3 > K_2 > K_1, as would be the case if the cratic contribution is the same and successively stronger enzyme to headgroup interactions occur in the complexes $E_3^{\#}$, $E_2^{\#}$, and $E_1^{\#}$. It is likely that the electrostatic (Coulombic) interactions contribute for the binding of the amphiphiles in $E_1^{\#}$. We believe the major contribution comes from the specific anion binding. Reducing the headgroup repulsion, the specific anion binding also desolvates the i-face to promote the hydrophobic segregation of the alkyl chains in $E_i^{\#}$. It is also possible that with fewer amphiphiles (as in the early complexes), the average headgroup to headgroup repulsion in the $E_i^{\#}$ complexes would be weaker than for the micelles.

The short-range specific anion-binding interactions (Figure 11B) along the i-face are expected to be stronger than the electrostatic effects. The estimated electrostatic contribution to PLA2 binding along the i-face is estimated to be about −1 kcal/mol (*11*, *25*, *42*, *43*). In the anion-assisted dimer of PLA2 (*30*−*32*), as well as in many other proteins (*44*), the specific binding of anions occurs through polarizable oxygen and nitrogen ligands. Involving the short-range specific anion binding in the amphiphile interaction with the i-face is consistent with the difference in the value of the *y*-intercept for the CMC versus K_1. The observed incremental contributions of about −0.5 kcal/mol per CH_2 suggests that the stability of $E_i^{\#}$ formed with the amphiphiles depends much more strongly on hydrophobic than on electrostatic effects. This linear extrapolation is based on the two assumptions: First, the hydrophobic effect prevails even at the short distances away from the sulfate headgroup, and second the exchange dynamics does not influence the dissociation constants. On the basis of the linearity of the plots in Figure 12, these two effects are apparently compensated for within the noise level of the results.

Hill Numbers. Assuming that there is an all-or-nothing amphiphile binding process, the Hill coefficients n_i describe the apparent number of cooperative sites involved in the formation of the complexes $E_i^{\#}$. Hill coefficients for the binding of alkyl sulfate homologues to $E_1^{\#}$ are between 1.4 and 2.8. It is consistent with the suggestion above that in the first step, three amphiphile molecules bind to each PLA2. Hill coefficients of 8 for the second step and of about 12 for the third step correspond to the binding of at least as many alkyl sulfate molecules per PLA2. Thus, the minimum effective number of amphiphiles associated with each $E_3^{\#}$ would be at least $3 + 8 + 12 \approx 23$. The actual number of bound amphiphiles per enzyme would be higher if the amphiphiles were to bind with less than total cooperativity. On the basis of the consideration of the depletion of amphiphiles for tight equilibrium binding (site-exclusion), it has been estimated that about 30−35 phospholipids bind to the i-face, an area of about 1650 A^2 (*6*, *11*, *13*−*16*, *30*−*32*).

As suggested above, the binding of the anions does not necessarily correspond to the stepwise binding of the five anions as seen in the dimer (Figure 11A). The three step sequential binding of amphiphiles to the i-face suggests that the overall amphiphile binding is "nucleated" in the first step by specific binding of some anionic headgroups. Binding of individual anions is also expected to be less steep if the hydrophobic sites preexisted on the i-face. As a result, cooperativity in each of the steps apparently results from the hydrophobic chain−chain packing interactions triggered by a decrease in the headgroup to headgroup repulsion between the amphiphiles bound to the i-face. Such a model raises the yet unexplored possibility that the equilibrium between the $E_i^{\#}$ species could depend on the nature of the headgroups. Furthermore, at the CMC and above, the relationships between the free E and the $E_i^{\#}$ complexes are determined by the ratios of CMC/K_i (eq 2 and 13). The near constancy of these ratios for different lengths of alkyl sulfate chains (Figure 12) suggests that in this limit, the equlibria between E and $E_i^{\#}$ are indeed determined primarily by interactions with or between headgroups.

Binding to Micelles and Self-Aggregation of $E_i^{\#}$. The self-aggregation of $E_i^{\#}$ and E* will influence the stability of the complexes and therefore the values of the primary parameters

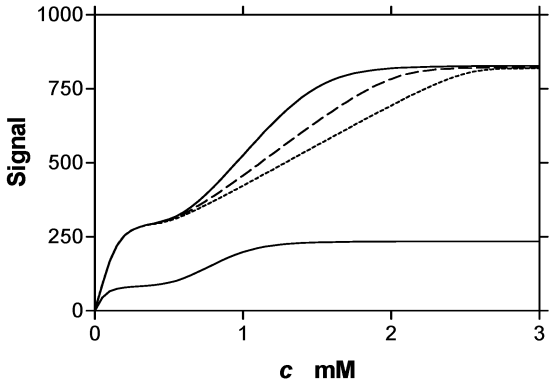

FIGURE 13: Expected behavior of a titration with decyl sulfate (C, mM) at different concentrations of E. Lowest curve is the best fit to the data for $E_T = 0.017$ mM in Figure 6 (with EGTA); at this enzyme concentration, the results are independent of amphiphile depletion. The upper three curves are the expected results at $E_T = 0.06$ mM: dotted $N_1 = 2$, $N_2 = 30$; dashed $N_1 = 2$, $N_2 = 20$; solid $N_1 = 2$, $N_2 = 10$.

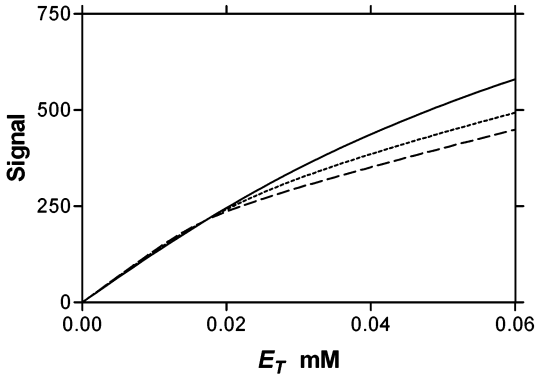

FIGURE 14: Predicted dependence of the signal as a function of added E (E_T, mM) at 1 mM decyl sulfate. This simulation is based on the parameter values in Figure 6 (with EGTA). Solid is for $N_1 = 2$, $N_2 = 10$; dotted is for $N_1 = 2$, $N_2 = 20$; dashed is for $N_1 = 2$, $N_2 = 30$. At these concentrations, the choice of N_1 makes little difference.

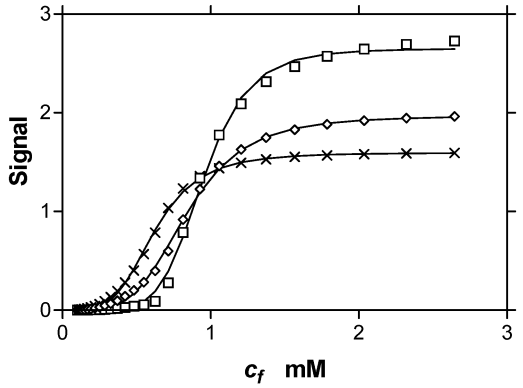

FIGURE 15: Influence from aggregate formation. Data points were generated with eqs 9 and 10, and the solid curves are the best fits with eq 11. Parameter values used for data generation in all cases: $E_T = 2$ μM, $K_{agg} = 0.8$ μM (which gives aggregation around $c_f = 1$ mM), $M = 10$, $n = 3$, $K = 1$ mM. Diamonds: $a_1 = a_2 = 1000$ gives best fit estimates $n = 4.3$, $K = 0.84$ mM. Squares: $a_1 = 200$, $a_2 = 2000$ gives best fit estimates $n = 6.1$, $K = 0.95$ mM. Crosses: $a_1 = 2000$, $a_2 = 200$ gives best fit estimates $n = 4.1$, $K = 0.62$ mM.

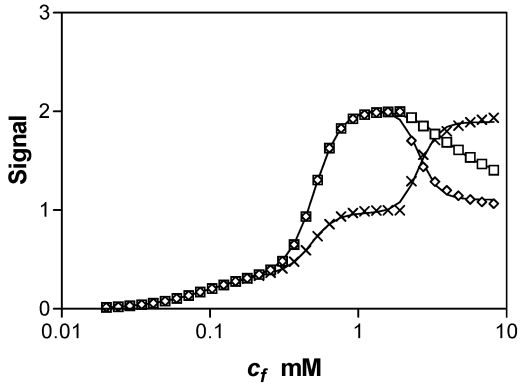

FIGURE 16: Effect of micellization on the E# complexation as a function of the free decyl sulfate concentration (C_f, mM). Data points were generated from eqs 13, 15, and 16 with $E_T = 0.002$ mM, CMC = 2 mM, $N = 200$, $n_1 = 2$, $K_1 = 0.1$, $a_1 = 200$, $n_2 = 5$, and $K_2 = 0.5$ mM. Diamonds: $a_2 = 1000$, $a_3 = 500$, and $K_d = 10^{-9}$ M. Squares: $a_2 = 1000$, $a_3 = 500$, and $K_d = 10^{-8}$ M. Crosses: $a_2 = 500$, $a_3 = 1000$, and $K_d = 10^{-9}$ M. The solid curves are the best fits to eq 4, neglecting the micellization above CMC. These best fits are $n_3 = 6.6$ and $K_3 = 2.6$ mM (diamonds and crosses) and $n_3 = 3.1$ and $K_3 = 4.0$ mM (circles).

(Table 1) that were calculated without regard to aggregation. Size-estimates from Figures 7−10 and Table 2 show that 100 to 1000 kDa aggregates are formed with PLA2 in the presence of monodispersed and micellar alkyl sulfate and DC$_n$PM-ether. This is both surprising and intriguing. Unfortunately, much of the structural information about the properties of premicellar $E_i^{\#}$ as well as the micellar E* is masked by the aggregates. For example, a relatively small difference between K_3 and CMC (Table 1 and Figure 12) suggests that K_3 is indeed an estimate of some real equilibrium constant and that the underlying process may be related to the aggregate formation. The level of uncertainty in the parameters for the formation of $E_3^{\#}$ is also larger because the signal is weak and the concentration range is small. For such reasons, the significance of the aggregation behavior can only be evaluated in qualitative terms. As developed in the Appendix (Section 2 and 3), there are at least four possible consequences of aggregation of $E_i^{\#}$:

(a) Self-aggregation of $E_2^{\#}$ or $E_3^{\#}$ (Section 2) would shift the equilibria from the previous steps and thus distort the measured fit parameters. Simulations in Figure 15 show that aggregate formation, as long as it does not involve the binding of extra amphiphiles not already present in E#, would not appear as a distinct step in the binding isotherm, making it difficult to establish its presence. The simulation results also depend strongly on how aggregation influences the intrinsic signal strength, if at all. However, as judged from the fit with the Hill equation, eq 11, aggregate formation does distort the curve somewhat, but mostly in a manner such that the estimated cooperativity for $E_i^{\#}$ formation, n_i, appears to be larger and the estimated dissociation constant appears to be smaller. The extent of aggregate formation is expected to increase with increasing enzyme concentration and may be insignificant at the low concentrations used in the spectroscopic experiments.

(b) In all cases (Table 1), K_3 is very similar to CMC, and $E_3^{\#}$ may correspond to the E* complex (Figure 1) that is formed by direct binding of E to preformed micelles (Appendix, Section 3). In Figure 16, we have simulated binding isotherms for E → $E_1^{\#}$ → $E_2^{\#}$ → E* and interpreted the results with the three Hill step model (i.e., with $E_3^{\#}$ instead of E*, eq 1). The value of K_3 estimated in this way

is always a little larger than CMC but depends also on the dissociation constant for E* to E, K_d; K_3 would be equal to CMC only if K_d were very small. The apparent high cooperativity (n_3) corresponds to a small K_d, yielding an estimated K_3 close to the amphiphile CMC (crosses and diamonds in Figure 16). From a modeling point of view, there are only very minor differences between the $E_3^{\#}$ vs E* description for the formation of the third complex (Figure 16). In fact, the results in Figure 3 could be fitted equally well using E* rather than $E_3^{\#}$ if the CMC values were 30, 3.2, and 0.13 mM for C_8SO_4, $C_{10}SO_4$, and $C_{12}SO_4$, respectively. As these numbers are consistently smaller than the measured CMC values (Table 1), we have chosen to discuss the results in terms of $E_3^{\#}$ as a distinct premicellar state.

(c) It is possible to form E* even below the CMC if the presence of $E_2^{\#}$ or $E_3^{\#}$ will help to nucleate micellization on the enzyme. This is not the same as saying that the presence of E lowers the CMC. Preliminary calculations (not shown) suggest that the effect of nucleation may be small: if CMC = 2 mM, E* could start to form at (say) 1.9 mM. The details of these relationships remain to be worked out.

(d) It is also possible that the $E_i^{\#}$ complexes "grow" with the binding of additional amphiphiles as they aggregate. This would significantly influence the effect of aggregation on the coupled equilibria. It could also make the aggregate stand out as a distinct premicellar species in the binding isotherms. One possibility is that $E_3^{\#}$ actually corresponds to an aggregate of $E_2^{\#}$ with more amphiphiles added in such a way that the complex resembles an aggregate of E*. A prediction from this scenario is that the value of K_3 would be smaller at high enzyme concentrations and would approach CMC at low enzyme concentrations.

Considering such possibilities for the course of aggregation of the $E_i^{\#}$ complexes, it is not trivial to satisfactorily interpret the difference between CMC and K_3. To explain the curves with E* replacing $E_3^{\#}$, we need very small values for K_d (Figure 16). This is not surprising since K_d is defined from the equilibrium between E and E*. Ignoring $E_3^{\#}$, if $E_2^{\#}$ dominates just below the CMC, the interesting equilibrium above the CMC would be between E* and $E_2^{\#}$ with the effective dissociation constant determined by

$$K_d(\mathrm{CMC}/K_1)^{n_1}(\mathrm{CMC}/K_2)^{n_2}$$

Similarly, monitoring only the micelle-bound enzyme (E*) versus all premicellar states (E, $E_1^{\#}$, $E_2^{\#}$) yields an effective dissociation constant, given by eq 17, which is substantially larger than K_d:

$$K_d^{\mathrm{eff}} = K_d\left\{1 + \left(\frac{\mathrm{CMC}}{K_1}\right)^{n_1}\left[1 + \left(\frac{\mathrm{CMC}}{K_2}\right)^{n_2}\right]\right\}$$

Equation 17 places some interesting limits with possible functional significance. In the absence of monodisperse amphiphiles (i.e., for very small CMC), K_d^{eff} would approach K_d. This is consistent with the observation that K_d^{eff} is considerably lower on bilayer vesicles than it is on micelles. However, one needs to be careful in using eq 17 in such comparisons. Although K_d describes the binding of the enzyme to a preformed interface, it is not necessarily the same for micelles as for bilayer vesicles. First, the organization and dynamics of the two kinds of interface are different: E* on bilayer does not change the bilayer organization, whereas the organization and aggregation of micellar E* is often different from that of micelles. Second, as discussed in the Appendix, the binding of E to micelles, but not to vesicles, could involve a number of extra amphiphiles that bind simultaneously. In this case, K_d for the micelles would also depend on the CMC as well as on the number of extra amphiphiles involved. As seen in Table 1 and Figure 12, there is also a covariation in K_i and CMC, such that the ratio CMC/K_i is nearly constant for alkyl sulfate chains of different lengths. Consequently, it is not meaningful to consider only the explicit dependence on CMC in eq 17 without accounting for concomitant difference in K_i and K_d. It can be expected that amphiphiles with very low CMC may also have very small K_i so that the competition from the premicellar states ($E_i^{\#}$) on the micellar binding may be of similar magnitude in many cases.

APPENDIX

1. Three-State Sequential Binding Below the CMC. Interpretation of some results in this paper requires that the binding of monodisperse amphiphile to enzyme below the CMC can take place in at least three different ways. We assume that the premicellar complexes ($E_i^{\#}$ in Figure 1) are formed in three steps through the sequential binding of N_1', N_2', and N_3' amphiphile molecules:

$$\mathrm{E} \underset{n_1,\,K_1}{\overset{+N_1'A}{\rightleftharpoons}} \mathrm{E_1}^{\#} \underset{n_2,\,K_2}{\overset{+N_2'A}{\rightleftharpoons}} \mathrm{E_2}^{\#} \underset{n_3,\,K_3}{\overset{+N_3'A}{\rightleftharpoons}} \mathrm{E_3}^{\#} \qquad (1)$$

Each binding step is described by the Hill parameter n_i and the dissociation constant K_i ($i = 1, 2, 3$). If [$E_i^{\#}$] denotes the concentration of complex $E_i^{\#}$, E_f the concentration of free enzyme, and c_f the concentration of free amphiphile, the equilibrium relations are

$$[\mathrm{E_1}^{\#}]/E_f = (c_f/K_1)^{n_1} \qquad (2a)$$

$$[\mathrm{E_2}^{\#}]/[\mathrm{E_1}^{\#}] = (c_f/K_2)^{n_2} \qquad (2b)$$

$$[\mathrm{E_3}^{\#}]/[\mathrm{E_2}^{\#}] = (c_f/K_3)^{n_3} \qquad (2c)$$

Thus, the total concentration of enzyme, E_T, must satisfy

$$E_f = \frac{E_T}{1 + (c_f/K_1)^{n_1}\{1 + (c_f/K_2)^{n_2}[1 + (c_f/K_3)^{n_3}]\}} \qquad (3)$$

Assuming that the signal from complex $E_1^{\#}$ is a_1, from complex $E_2^{\#}$ is a_2, and from complex $E_3^{\#}$ is a_3, the total signal can be expressed as

$$S(E_T, c_f) = E_T\frac{(c_f/K_1)^{n_1}\{a_1 + (c_f/K_2)^{n_2}[a_2 + a_3(c_f/K_3)^{n_3}]\}}{1 + (c_f/K_1)^{n_1}\{1 + (c_f/K_2)^{n_2}[1 + (c_f/K_3)^{n_3}]\}} \qquad (4)$$

When amphiphile is in large excess over enzyme, the depletion of free amphiphile due to the complex formation can be neglected and c_f in eq 4 can be replaced by the total concentration c. If the three binding steps are well separated, the nine parameters n_1, n_2, n_3, K_1, K_2, K_3, a_1, a_2, and a_3 can

be estimated. If only two binding steps contribute, the result is given by eq 4 but with $1/K_3$ set to zero.

When amphiphile is not in large excess over enzyme, depletion becomes important. Assuming that $N_1 = N_1'$, $N_2 = N_1' + N_2'$, and $N_3 = N_1' + N_2' + N_3'$ amphiphiles are bound in complex $E_i^{\#}$ ($i = 1, 2, 3$), the concentration, c_f, of free amhiphiles can be solved numerically from

$$E_T = \frac{(c - c_f)\{1 + (c_f/K_1)^{n_1}\{1 + (c_f/K_2)^{n_2}[1 + (c_f/K_3)^{n_3}]\}\}}{(c_f/K_1)^{n_1}\{N_1 + (c_f/K_2)^{n_2}[N_2 + N_3(c_f/K_3)^{n_3}]\}} \quad (5)$$

Inserting the result from eq 5 into eq 4 gives the signal as a function of the total concentrations c and E as determined by the 12 parameters N_1, N_2, N_3, n_1, n_2, n_3, K_1, K_2, K_3, a_1, a_2, and a_3. Unless some parameters are known from other results, the stoichiometry factors, N_1, N_2, and N_3, cannot easily be determined from these results. The primary effect of depletion will be to distort the curves, making the cooperativity, n_i, appear to be smaller and the dissociation constant, K_i, appear to be larger as shown in Figure 13. The effect of depletion on the titration of decyl sulfate with E is shown in Figure 14.

2. Influence of E# Aggregation. Consider the reaction

$$E \overset{n,K}{\longleftrightarrow} E^{\#} \overset{K_{agg}}{\longleftrightarrow} (E^{\#})_{agg} \quad (6)$$

Here, the first step is the cooperative binding of amphiphiles to form the complex $E^{\#}$, and the second step is the aggregate formation of M $E^{\#}$-complexes (see Figure 1). Assuming that the free concentration of amphiphile in solution is c_f, the equilibrium concentrations will satisfy the relations

$$[E^{\#}] = E_f(c_f/K)^n \quad (7)$$

$$[(E^{\#})_{agg}] = K_{agg}([E^{\#}]/K_{agg})^M \quad (8)$$

In eq 8, the aggregate is defined as an all-or-nothing joining of M $E^{\#}$-complexes. The equilibrium constant, K_{agg}, defined in this way will have the units of concentration. Equation 8 also assumes that aggregation does not involve the binding of extra amphiphile molecules that are not already present in $E^{\#}$. If aggregation involves the extra binding of m amphiphiles with a dissociation constant K_a, eq 8 would have an extra factor $(c_f/K_a)^m$ on the right-hand side. The concentration, E_f, of free enzyme, i.e., enzyme in state E, can be determined numerically from

$$E_T = E_f\left[1 + \left(\frac{c_f}{K}\right)^n\right] + MK_{agg}\left(\frac{c_f}{K}\right)^{nM}\left(\frac{E_f}{K_{agg}}\right)^M \quad (9)$$

If the signal from $E^{\#}$ is a_1 and from $(E^{\#})_{agg}$ is a_2, the total signal will be

$$S = a_1E_f\left(\frac{c_f}{K}\right)^n + a_2MK_{agg}\left(\frac{c_f}{K}\right)^{nM}\left(\frac{E_f}{K_{agg}}\right)^M \quad (10)$$

where E_f is determined from eq 9. If the concentration of amphiphile is much larger than that of enzyme, the free concentration c_f in eqs 9 and 10 can be approximated by the total, c.

The result, if there is no aggregation, will be the Hill equation

$$S = \frac{a_1E_T(c_f/K)^n}{1 + (c_f/K)^n} \quad (11)$$

We have used eqs 9 and 10 to generate hypothetical data from the scheme in eq 6. Then, these data were analyzed with eq 11 as if aggregate formation did not occur. Some results are shown in Figure 15. The main result is that aggregate formation does not show up as a distinct phase in the signal, as long as aggregation does not involve extra amphiphile binding, which makes it difficult to determine its presence. However, as judged from the fit with eq 11, aggregate formation does distort the curve somewhat, but mostly in a way so that the estimated cooperativity for $E^{\#}$ formation, n, is larger and the estimated dissociation constant, K, is smaller. Aggregation depends on the amount of enzyme present, and at sufficiently low enzyme concentrations, aggregates will not form. The results also depend strongly on how aggregation influences the signal strength, if at all.

3. Influence of Micellization. Some results suggest that the third state, $E_3^{\#}$ in the scheme of eq 1, actually corresponds to E*, i.e., enzyme bound to micelle (Figure 1). If so, we can consider an alternative three-stage binding scheme

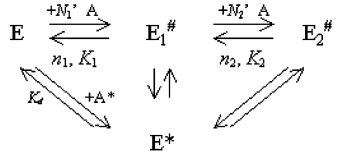

(12)

In this scheme, the dissociation constant K_d is defined from the equilibrium between E and E*. However, E* may well form from $E_2^{\#}$ or $E_1^{\#}$, and the corresponding dissociation constants are defined by detailed balance in the scheme of eq 12: e.g., $[E_2^{\#}]/[E^*] = (K_d/m_f)(c_f/K_1)^{n_1}(c_f/K_2)^{n_2}$, where m_f is the concentration of micellar amphiphiles available for enzyme binding (see eq 14 below). If enzyme binding stabilizes the micelle, it is possible that the binding of E to E* also involves a growth of the micelle through the addition of a few extra amphiphiles. If m extra amphiphiles are bound in this way, we would expect that the corresponding dissociation constant K_d is proportional to $(c_f)^{-m}$. Thus, if m is the same as the number, $n_1 + n_2$, of amphiphiles carried by $E_2^{\#}$, the equilibrium between $E_2^{\#}$ and E* would be independent of c_f. If $E_3^{\#}$ is different from E*, it is straightforward to include the extra state $E_3^{\#}$ in the scheme of eq 12 and in the equations that follow.

When micellization occurs above CMC, the concentration of free amphiphile in solution, c_f, can be expressed as

$$c_f = \begin{cases} c; \text{ if } c < \text{CMC} \\ \text{CMC}; \text{ if } c \geq \text{CMC} \end{cases} \quad (13)$$

where c is the total concentration of added amphiphile. Similarly, the concentration of micellar amphiphile that is available for binding of E, m_f, is (*5*):

$$m_f = \begin{cases} 0; c \leq \text{CMC} \\ \dfrac{c - \text{CMC}}{1 + NE_f/K_d}; c > \text{CMC} \end{cases} \quad (14)$$

N is a site-exclusion parameter that accounts for the number of amphiphiles that are "covered" by each bound enzyme and not available for further binding. It may be primarily a fitting parameter. In this formulation it is assumed that $c \gg E_T$, so that the amount of amphiphiles that are bound in the $E_i^{\#}$ complexes can be neglected relative to c. The concentration of free enzyme, E_f, can be determined from a second-degree equation given by

$$E_T = E_f\left\{1 + \left(\frac{c_f}{K_1}\right)^{n_1}\left[1 + \left(\frac{c_f}{K_2}\right)^{n_2}\right] + \frac{c - \mathrm{CMC}}{K_d + NE_f}\right\} \quad (15)$$

If the signals from the three states, $E_1^{\#}$, $E_2^{\#}$ and E*, are a_1, a_2 and a_3, respectively, the total signal will be

$$S = E_f\left\{\left(\frac{c_f}{K_1}\right)^{n_1}\left[a_1 + a_2\left(\frac{c_f}{K_2}\right)^{n_2}\right] + a_3\frac{c - \mathrm{CMC}}{K_d + NE_f}\right\} \quad (16)$$

In eqs 15 and 16, the term involving $c - \mathrm{CMC}$ contributes only for $c >$ CMC and should be set equal to zero for $c <$ CMC. This result can be compared with the results from the three-step scheme in eq 1 that does not include micellization. The two schemes cannot be easily distinguished from the shape of the corresponding curves. If the $E_3^{\#}$ state is interpreted as E* in eq 1, the estimated cooperativity, n_3, will be inversely related to K_d (see Figure 16) and would have no meaning as a stoichiometry parameter. The results show that the curves are virtually indistinguishable if we incorporate aggregation (Figure 15) or micellization (Figure 16). Only the interpretation of parameters will change.

It should be reemphasized that K_d is defined as the equilibrium between E and E*. If we are interested in the micellar binding, E*, in relation to all the solution states (E, $E_1^{\#}$, and $E_2^{\#}$), the effective dissociation constant is

$$K_d^{\mathrm{eff}} = K_d\left\{1 + \left(\frac{\mathrm{CMC}}{K_1}\right)^{n_1}\left[1 + \left(\frac{\mathrm{CMC}}{K_2}\right)^{n_2}\right]\right\} \quad (17)$$

As discussed above, the dissociation constant K_d will also depend on CMC if extra amphiphiles are involved in the E to E* step. In principle, the existence of the premicellar states, $E^{\#}$, will destabilize the micellar binding compared to a situation where they do not contribute (if K_1, $K_2 \gg$ CMC). However, K_1 and K_2 involve interactions similar to those of both CMC and K_d, and it may not be meaningful to compare situations where only some of the parameters are different.

REFERENCES

1. Berg, O. G., and Jain, M. K. (2001) *Interfacial Enzyme Kinetics*, p 302, Wiley & Sons, New York.
2. Berg, O. G., Tsai, M. D., Gelb, M. H., and Jain, M. K. (2001) Interfacial Enzymology: The secreted phospholipase A_2-paradigm, *Chem. Rev. 101*, 2613−2653.
3. Verheij, H. M., Slotboom, A. J., and de Haas, G. H. (1981) Structure and Function of Phospholipase A_2, *Rev. Physiol. Biochem. Pharmacol. 91*, 91−203.
4. Yu, B. Z., Apitz-Castro, R., Tsai, M. D., and Jain, M. K. (2003) Interaction of monodisperse anionic amphiphiles with the i-face of secreted phospholipase A_2, *Biochemistry 42*, 6293−6301.
5. Berg, O. G., Yu, B. Z., Apitz-Castro, and Jain, M. K. (2004) PI-specific phospholipase C forms different complexes with monodisperse and micellar phosphatidylcholine, *Biochemistry 43*, 2080−2090.
6. Jain, M. K. Egmond, M. R., Verheij, H. M., Apitz-Castro, R. J., Dijkman, R., and de Haas, G. H. (1982) Interaction of phospholipase A_2 and phospholipid bilayers, *Biochim. Biophys. Acta 688*, 341−348.
7. Apitz-Castro, R. J., Jain, M. K., and de Haas, G. H. (1982) Origin of the latency phase during the action of phospholipase A_2 on unmodified phosphatidylcholine vesicles, *Biochim. Biophys. Acta 688*, 349−356.
8. Jain, M. K., Ranadive, G. N., Rogers, J. M., Yu, B. Z., Berg, O. G. (1991) Interfacial catalysis by phospholipase A_2: Dissociation constants for calcium, substrate, products, and competitive inhibitors, *Biochemistry 30*, 7306−7317.
9. Yu, B. Z., Berg, O. G., Jain, M. K. (1993) The divalent cation is obligatory for the binding of ligands to the catalytic site of secreted phospholipase A_2, *Biochemistry 32*, 6485−6492.
10. Berg, O. G., Rogers, J. M., Yu, B. Z., Yao, J., Romsted, L. S., and Jain, M. K. (1997) Thermodynamic and kinetic basis for interfacial activation: Resolution of binding and allosteric effects on pancreatic phospholipase A_2 at zwitterionic interfaces, *Biochemistry 36*, 14512−14530.
11. Ramirez, F., and Jain, M. K. (1991) Phospholipase A_2 at the bilayer interface, *Proteins 9*, 229−239.
12. Yu, B. Z., Janssen, M. J. W., Verheij, H. M., and Jain, M. K. (2000) Control of the chemical step by leucine-31 of pancreatic phospholipase A_2, *Biochemistry 39*, 5702−5711.
13. De Araujo, P. S., Rossneu, M. Y., Kremer, J. M. H., van Zolen, E. H., de Haas, G. H. (1979) Structure and thermodynamic properties of the complexes between phospholipase A_2 and lipid micelles, *Biochemistry 18*, 580−586.
14. Hille, J. D. R., Donne-Op den Kelder, G., Sauve, M., de Haas, G. H., and Egmond, M. R. (1981) Physicochemical studies on the interaction of pancreatic phospholipase A_2 with micellar substrate analogue, *Biochemistry 20*, 4068−4073.
15. Van Oort, M. G., Dijkman, R., Hille, J. D. R., and de Haas, G. H. (1985) Kinetic behavior of porcine pancreatic phospholipase A_2 on zwitterionic and negatively charged single-chain substrates, *Biochemistry 24*, 7987−93.
16. Van Oort, M. G., Dijkman, R., Hille, J. D. R., and de Haas, G. H. (1985) Kinetic behavior of porcine pancreatic phospholipase A_2 on zwitterionic and negatively charged double-chain substrates, *Biochemistry 24*, 7993−99.
17. Jain, M. K., and Rogers, J. M. (1989) Substrate specificity for interfacial catalysis by phospholipase A_2 in the scooting mode, *Biochim. Biophys. Acta 1003*, 91−32.
18. Rogers, J., Yu, B. Z., and Jain, M. K. (1992) Basis for the anomalous effect of competitive inhibitors on the kinetics of hydrolysis of short chain phosphatidylcholines by phospholipase A_2, *Biochemistry 31*, 6056−6062.
19. Rogers, J., Yu, B. Z., Serves, S. V., Tsivgoulis, G. M., Sotiropoulos, D. N., Ioannou, P. V., and Jain, M. K. (1996) Kinetic basis for the substrate specificity during hydrolysis of phospholipids by secreted phospholipase A_2, *Biochemistry 35*, 9375−84.
20. Deveer, A. M. T. J., den Ouden, A. T., Gallay, V. M., Verger, R., Egmond, M. R., Verheij, H. M., and de Haas, G. H. (1992), *Biochim. Biophys. Acta 1126*, 95−102.
21. Homan, R. and Jain, M. K. (2000) Biology, pathology and interfacial enzymology of pancreatic phospholipase A_2. In *Intestinal Lipid Metabolism* (Mansbach, C. M., Tso, P., and Kuksis, A., Eds.), pp 81−104, Kluwer Academic Press−Plenum, New York.
22. Jain, M. K., Rogers, J., Jahagirdar, D. V., Marecek, J. F., Ramirez, F. (1986) Kinetics of interfacial catalysis by phospholipase A_2 in intravesicle scooting mode, and heterofusion of anionic and zwitterionic vesicles, *Biochim. Biophys. Acta 860*, 435−447.
23. Berg, O. G., Yu, B. Z., Rogers, J., Jain, M. K. (1991) Interfacial catalysis by phospholipase A_2: Determination of the interfacial kinetic rate constants, *Biochemistry 30*, 7283−7297.
24. Jain, M. K., Ranadive, G. N., Yu, B.-Z., and Verheij, H. M. (1991) Interfacial catalysis by phospholipase A_2: Monomeric enzyme is fully catalytically active at the bilayer interface, *Biochemistry 30*, 7330−7340.
25. Rogers, J. M., Yu, B. Z., Tsai, M. D., Berg, O. G., and Jain, M. K. (1998) Cationic residues 53 and 56 control the anion-induced interfacial k^*_{cat}-activation of pancreatic phospholipase A_2, *Biochemistry 37*, 9549−9556.
26. Yu, B. Z., Poi, M. J., Ramagopal, U. A., Jain, R., Ramakumar, S., Berg, O. G., Tsai, M. D., Sekar, K., and Jain, M. K. (2000)

Structural basis of the anionic interface preference and k^*_{cat}-activation of pancreatic phospholipase A_2, *Biochemistry 39*, 12312−23.
27. Van Eijk, J. H., Verheij, H. M., Dijkman, R., and De Hass, H. G. (1983). Interaction of phospholipase a2 from Najamelanoleuca snake venom with monomeric substrate analogues. Activation of the enzyme by protein−protein or lipid−protein intercations? *Eur. J. Biochem. 132*, 183−188.
28. Pan, Y. H., Yu. B.-Z., Singer, A. G., Ghomashchi, F., Lambeau, G., Gelb, M. H., Jain, M. K., Bahnson, B. J. (2002) Crystal structure of human group X secreted phospholipase A_2: Electrostatically neutral interfacial binding surface targets zwitterionic membranes, *J. Biol. Chem. 277*, 20986−93.
29. Boegman, S. C., Deems, D. A., and Dennis, E. A. (2004) Phospholipid binding and activation of group IA secreted phospholipase A_2. *Biochemistry 43*, 3907−1916.
30. Pan, Y. H., Epstein, T. M., Jain, M. K., and Bahnson, B. J. (2001) Five coplanar anion binding sites on one face of phospholipase A_2: Relationship to interface binding, *Biochemistry 40*, 609−617.
31. Jain, M. K., Rogers, J., Hendrickson, H. S., Berg, O. G. (1993) The chemical step is not rate-limiting during the hydrolysis by phospholipase A_2 of mixed micelles of phospholipid and detergent *Biochemistry 32*, 8360−8367.
32. Epstein, T. M., Yu, B.-Z., Pan, Y. H., Tutton, S. P., Maliwal, B. P., Jain, M. K., and Bahnson, B. J. (2001) The basis for k^*_{cat}-impairment in phospholipase A_2 from the anion-assisted dimer structure, *Biochemistry 40*, 11411−11422.
33. Pan, Y. H., Yu, B. Z., Berg, O. G., Jain, M. K., Bahnson, B. J. (2002) Crystal structure of phospholipase A_2 complex with the hydrolysis products of platelet activating factor: Equilibrium binding of fatty acid and lysophospholipid-ether at the active site may be mutually exclusive, *Biochemistry 41*, 14790−8000.
34. Jain, M. K., Yu, B.-Z., and Berg, O. G. (1993) Relationship of interfacial equilibria to interfacial activation of phospholipase A_2, *Biochemistry 32*, 11319−11329.
35. Jain, M. K., Maliwal, B. P., de Haas, G. H., and Slotboom, A. J. (1986) Anchoring of phospholipase A_2: the effect of anions and deuterated water, and the role of N-terminus region, *Biochim. Biophys. Acta 860*, 448−461.
36. Jain, M. K. and Maliwal, B. P. (1993) Spectroscopic properties of the states of pig pancreatic phospholipase A_2 at interfaces and their possible molecular origin, *Biochemistry 32*, 11838−11846.
37. Yu, B. Z., Rogers, J., Nicol, G., Theopold, K. H., Seshadri, K., Vishweshwara, S., and Jain, M. K. (1998) Catalytic significance of the specificity of divalent cations as K_S^* and k^*_{cat} cofactor for secreted phospholipase A_2, *Biochemistry 37*, 12576−87.
38. Yu, B. Z., Ghomashchi, F., Cajal, Y., Annand, R. R., Berg, O. G., Gelb, M. H., and Jain, M. K. (1997) Use of an imperfect neutral diluent and outer vesicle layer scooting mode hydrolysis to analyze the interfacial kinetics, inhibition, and substrate preferences of bee venom phospholipase A_2, *Biochemistry 36*, 3870−3881.
39. Tanford, C. (1980) *Hydrophobic Effect*, Wiley, New York.
40. Cevec, G., and Marsh, D. (1987) *Phospholipid Bilayers: Physical Principles and Models*, Wiley, New York, p 442.
41. Dill, K. A., Koppel, D. E., Cantor, R. S., Dill, J. D., Bendedouch, D., and Chen, S. H. (1984) Molecular conformations in surfactant micelles, *Nature 309*, 42−45.
42. Lin, Y., Ghomashchi, F., Nielson, R., Snitko, Y., Yu, B. Z., Han, S. K., Cho, W., Wilton, D. C., Jain, M. K., Robinson, B. H., and Gelb, M. H. (1998) Binding of bee venom and human group IIa phospholipase A_2 to membranes: A minor role for electrostatics, *Biochem. Soc. Trans. 26*, 341−345.
43. Koduri, R. S., Baker, S. F., Snitko, T., Han, S. K., Cho, W., Wilton, D. C., Gelb, M. H. (1998) Action of human group IIa secreted phospholipase A_2 on cell membranes. Vescicle but not heparinoid binding determines rate of fatty acid release by exogeneously added enzyme, *J. Biol. Chem. 273*, 32142−49.
44. Chakrabarti, P. (1993) Anion binding sites for protein structures, *J. Mol. Biol. 234*, 463−482.

BI0497650